

Multicritical Fermi surface topological transitions

Dmitry V. Efremov^{1,2,*}, Alex Shtyk^{3,*}, Andreas W. Rost^{4,5,#}, Claudio Chamon⁶, Andrew P. Mackenzie^{4,7}, and Joseph J. Betouras^{1,#}

¹ Department of Physics, Loughborough University,
Loughborough LE11 3TU, UK.

² Leibniz-Institute for Solid State and Materials Research,
IFW-Dresden, D-01171 Dresden, Germany.

³ Department of Physics, Harvard University,
Cambridge, MA 02138, USA

⁴ School of Physics and Astronomy,
University of St Andrews, UK

⁵ Max Planck Institute for Solid State Research,
Heisenbergstr. 1, 70569 Stuttgart, Germany.

⁶ Department of Physics, Boston University,
Boston, MA, 02215, USA.

⁷ Max Planck Institute for Chemical Physics of Solids,
Noethnitzer Strasse 40, 01187 Dresden, Germany.

* These authors contributed equally.

Corresponding authors: J.Betouras@lboro.ac.uk; a.rost@st-andrews.ac.uk
(Dated: July 31, 2022)

A wide variety of complex phases in quantum materials are driven by electron-electron interactions, which are magnified by regions in momentum space where the density of states is enhanced. A well known example occurs at van Hove singularities where the Fermi surface undergoes a topological transition. Here we show that higher order singularities, where multiple disconnected leafs of Fermi surface touch all at once, naturally occur at points of high symmetry in the Brillouin zone. Such multicritical singularities can lead to stronger divergences in the density of states than canonical van Hove singularities, and further boost the formation of complex quantum phases via interactions. As a concrete example, we demonstrate these theoretical ideas in the analysis of experimental data on $\text{Sr}_3\text{Ru}_2\text{O}_7$ in the vicinity of the metamagnetic quantum critical point, resolving several previously puzzling aspects of the data.

Introduction. The properties of unconventional density waves in quantum materials are generally connected to features of the electronic band structure. Characteristic wave vectors of emergent order parameters can for example often be related to nesting-type features of the underlying Fermi surface as discussed for e.g. iron pnictides¹, organics², and transition metal dichalcogenides³. Yet these nesting features in themselves usually cannot account for the observed thermodynamic stability of such correlated quantum phases. Intriguingly in a range of these materials the band structure hosts energetically close-by singularities in the density of states (DOS), which have been conjectured to be crucial ingredients stabilising the emergent phases.

Singularities in the DOS occur naturally at Fermi surface (FS) topological Lifshitz transitions (LT). A prominent example is the van Hove singularity (vHs) formed at a saddle point in the energy-momentum dispersion (see fig. 1a). A two-dimensional (2D) vHs has a relatively weak logarithmic divergence in the DOS but is known to lead to a wealth of phenomena such as ferromagnetism driven by the Stoner mechanism (see eg. Ref. 4). An important yet under-appreciated point is that the thermodynamic stability of the emergent phases does not only depend on the magnitude but also shape of the singularity as a function of energy⁴ (i.e. gradient and curvature). As a consequence stronger power law divergences can have a much more dramatic impact on the formation of complex ordered phases than the relatively weak vHs.

Building on this insight, we explore a generalisation of these concepts to multicritical topological transitions where multiple disjoint parts of a FS merge. Such multicritical FS topological transitions naturally occur at points of high crystal symmetry, where the number n of FS components merging depends on the particular symmetry. In fig. 1a-c we illustrate the symmetries associated with the $n = 2$ (vHs), 3 and 4 cases in 2D. When the singularity occurs at an edge of a Brillouin zone there are generically two pieces ($n = 2$) of the Fermi surface that join at the singularity, as depicted in fig. 1a. The red lines are Fermi surface contours above and below the singularity. At the critical energy (dotted line) there is a topology change in the Fermi surface structure with $n = 2$ Fermi surfaces touching and reconnecting. At the corner of a hexagonal Brillouin zone, three Fermi surfaces or leaves ($n = 3$) can join at the singularity, as happens in e.g. biased bilayer graphene²⁰, (fig. 1b). In the square lattice, four leaves ($n = 4$) can meet at the X -point in the corner of the Brillouin zone (fig. 1c). At these high symmetry points higher order terms in the dispersion can become relevant, critically changing the nature of the divergence in the DOS, as for the power-law

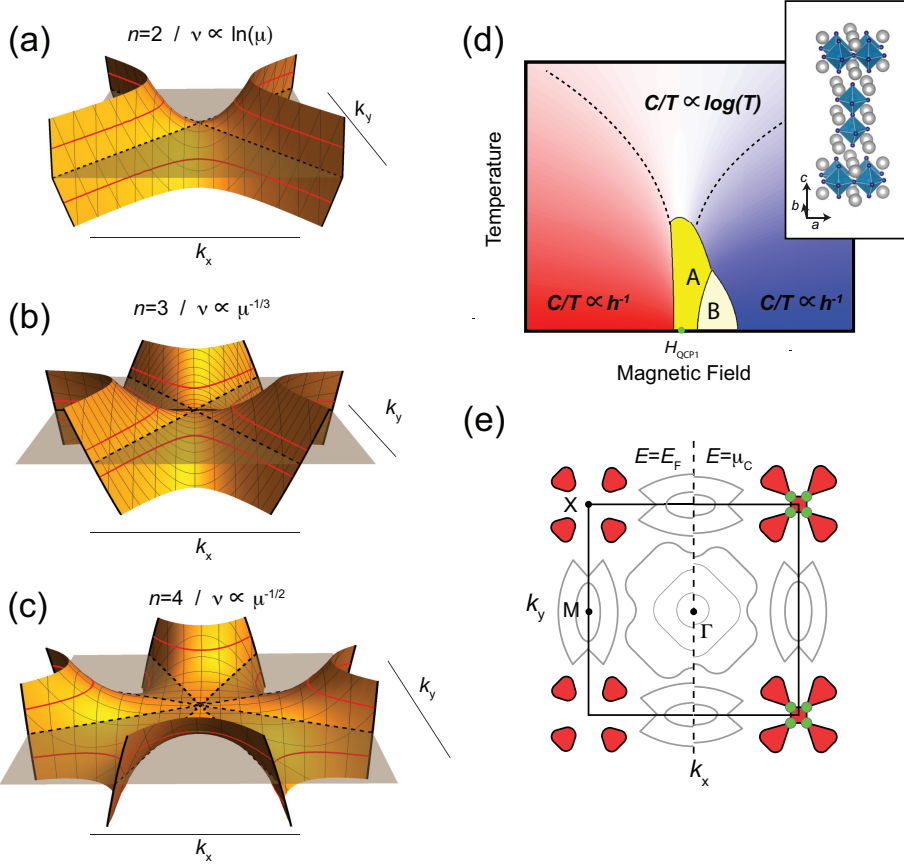


Figure 1: (a) The $n=2$ 2D van Hove singularity in the form of a saddle point. The density of states ν diverges as $\ln \mu$. Red lines indicate Fermi surfaces above and below the singularity. The critical Fermi surface is shown by the dotted black line. (b,c) The $n = 3, 4$ singularities at other high symmetry points. (d) Schematic phase diagram of $\text{Sr}_3\text{Ru}_2\text{O}_7$ together with the crystal structure shown in the inset⁶. The inset shows the crystal structure. Bilayers of RuO octahedra (blue) are separated by Sr spacer layers (gray). (e) Schematic of the quasi-2D Fermi surface of $\text{Sr}_3\text{Ru}_2\text{O}_7$ in the $k_z=0$ plane at the Fermi energy (left hand side) and at μ_c (right side). The crucial bands are highlighted in red. The main difference seen in the vicinity of the X point. At the critical chemical potential four close-by Lifshitz transitions (green) are forming close to the X-point connecting the existing hole-like Fermi surface with a new emerging small pocket at the centre. In order to emphasise the characteristic clover leaf Fermi surface we show an extended k -space picture beyond the Brillouin zone boundaries.

divergence in the $n=4$ case discussed below.

In order to provide an explicit example for these concepts we examine the layered perovskite $\text{Sr}_3\text{Ru}_2\text{O}_7$, which has been intensely studied because of its unusual magnetic and transport properties⁶. We identify a strong $n = 4$ power-law singularity at a four-fold symmetric point in momentum space and demonstrate how, in conjunction with other features of the FS and strong electron interactions, it is pivotal for the physical properties of this material, explaining several previously perplexing characteristics.

The central feature of its magnetic phase diagram is a metamagnetic quantum critical end point (QCEP) located at $H_C=8$ T for fields parallel to the crystallographic c -axis⁷ (Fig. 1d). The strong electron correlations related to this QCEP are evident in thermodynamic properties. The magnetic susceptibility is strongly enhanced (Wilson ratio of 10), consistent with $\text{Sr}_3\text{Ru}_2\text{O}_7$ being on the border of ferromagnetism⁸, achievable by modest uniaxial pressure⁹.

Approaching H_c as a function of T , a logarithmic divergence in specific heat divided by temperature C/T is observed¹⁰. Away from the critical field, a crossover to a low temperature Fermi liquid regime occurs¹¹. The approach to H_c as a function of magnetic field in the Fermi liquid regime is characterised by a singular contribution to C/T . Careful analysis¹² reveals a power law divergence of C/T as a function of reduced field $h = (H - H_C)/H_C$ with an unexpected exponent of -1. It has been suggested that the singularities in C/T as a function of field or temperature are consistent with a 2D metamagnetic QCEP within the canonical description of quantum criticality¹³. The expected exponent within this theoretical framework is -1/3 and in general has to be fixed in any fit of this model¹⁴. The observed

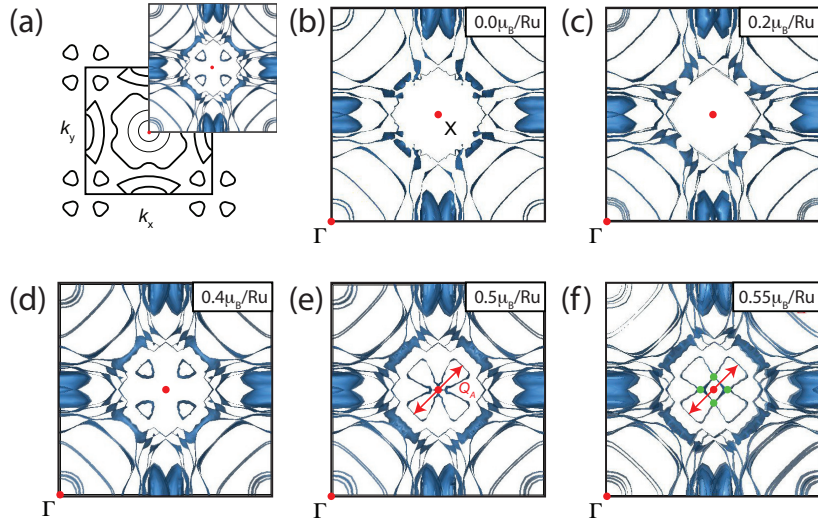


Figure 2: Result of the DFT calculation. (a) Here we show the schematic Fermi surface structure from Fig. 1e together with the k_z -projected DFT calculation to aid orientation. (b-f) Projected Fermi surfaces for values of magnetization $\mu=0.0, 0.2, 0.4, 0.5, 0.55 \mu_B$ per unit cell as calculated by the density functional method and centered at the X point. The topological transitions are evident for the value of magnetization close to $0.5 \mu_B$ and $0.55 \mu_B$ per unit cell. The red arrow in (e,f) connects the two nested parts of the characteristic clover leaf structure giving rise to the density wave in the A-phase.

exponent of -1 in an assumption-free power law fit to C/T therefore raises the important question of whether the current theoretical understanding is incomplete.

At low temperature, access to the QCEP is preempted by an unusual set of emergent phases (labelled A, B in Fig. 1d)¹⁵. Due to the observed anisotropic conductivities these have been referred to as “electron nematics”¹⁵. More recent neutron scattering measurements¹² revealed in addition an incommensurate magnetic order with a wave vector $\vec{Q}^A = (\pm 0.233, 0, 0) / (0, \pm 0.233, 0)$ and $\vec{Q}^B = (\pm 0.218, 0, 0) / (0, \pm 0.218, 0)$ respectively. Lester *et al.*¹² note that the observed Q -vectors might be related to FS nesting including the γ band centered at the X-point central to the theory developed below. Surprisingly, the entropy of the magnetically ordered A phase is higher than that of the adjacent low field phase¹².

The electronic band structure in the low field Fermi Liquid has been extensively studied experimentally^{8,10,11}. The layered crystal structure gives rise to an effectively 2D Fermi surface. In Fig. 1e we show schematically the key features both at the Fermi energy E_F as well as at an elevated energy E_{LT} . At the latter there is an $n = 4$ Lifshitz transition (LT) point occurring at the X-point of the Brillouin zone as becomes apparent by the characteristic clover leave structure in the extended zone (compare to Fig. 1c).

In the present work we identify the nontrivial power law singularity in the DOS of this $n = 4$ LT as the essential feature underlying the observed phenomena including several previously puzzling features. In particular, we (i) account for key thermodynamic properties approaching the critical region, (ii) the formation of the SDW out of the (quantum) critical normal phase and (iii) entropy changes associated with entering the A-phase by increasing magnetic field.

Fermi Surface as calculated by DFT. To understand the origin of the singularity in the DOS we performed density functional theory (DFT) calculations of the electronic structure. The calculated band structure for zero magnetization agrees broadly with ARPES data⁸ (Fig. 2a). While the chemical potential is slightly higher than observed experimentally this does not affect the key conclusions drawn here. We therefore considered the evolution of the DOS with increasing magnetic moment per unit cell (see Fig. 2), as a convenient way to model the effects of an externally applied magnetic field. The calculated FS topology for zero magnetisation agrees broadly with ARPES data⁸. By increasing the magnetic moment the LT is observed at the X-point at magnetization around $0.5 \mu_B/\text{Ru}$. This topological transition is the dominant feature in the thermodynamic properties due to an associated power law increase in the DOS. The characteristic clover leaf structure of the Fermi surfaces in the vicinity of the LT naturally gives rise to strong nesting of the edges of the γ -bands which, in addition to the multicritical LT, helps generate the SDW. It is important to note that the nested Fermi surface parts have a distinct orbital character from the multicritical LT. The value of the nesting vector $\vec{Q} = (\pm 0.23, 0, 0)$ or $(0, \pm 0.23, 0)$ is effectively that observed experimentally in phase A.

Given the strong electron correlations, DFT calculations cannot capture all properties such as Fermi velocities accurately. We therefore set up a tight binding model based on the Ru 4d orbitals (see Supplemental Information)

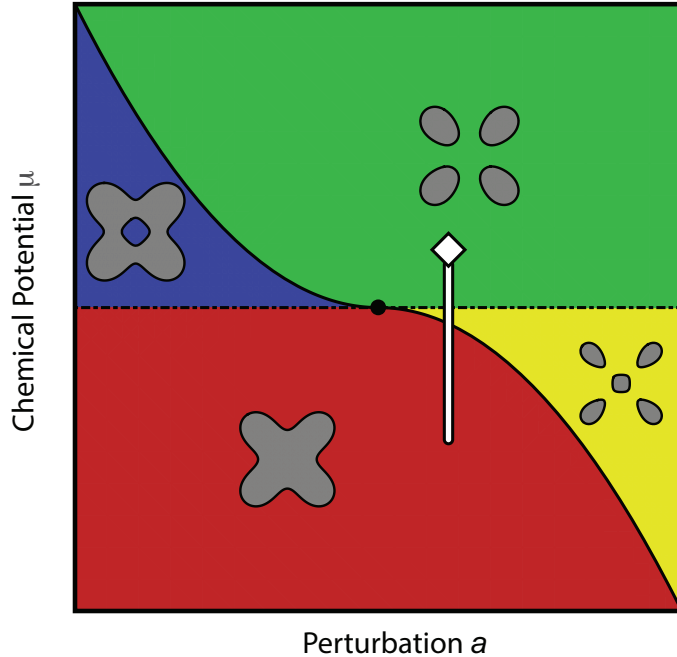


Figure 3: Topological phase diagram of the relevant hole-like version of the effective dispersion relation (1). In $\text{Sr}_3\text{Ru}_2\text{O}_7$ there is no control over the parameter $a > 0$, so that only red, yellow and green phases are accessible. There are two lines of LTs, a dashed-dotted line of a band edge type and a solid line corresponding to the transition of the neck-narrowing type. The X_9 singularity is located at the crossing of these two lines. The white line schematically shows the location of $\text{Sr}_3\text{Ru}_2\text{O}_7$ within this phase diagram with the diamond marking schematically the location in zero field.

relevant at the Fermi energy¹. This allows the identification of essential ingredients generating the multicritical Lifshitz point and crucially adjustment of the tight binding parameters to accurately describe the relevant part of the ARPES data. The results based on the effective low energy Hamiltonian agree with the DFT calculations with respect to both the occurrence of the multicritical LT and the formation of the SDW.

Effective dispersion relation and analysis. The dispersion in the vicinity of the multicritical Lifshitz point can be approximated by the simple dispersion relation

$$\varepsilon(\vec{k}) = \begin{cases} ak^2 + k^4 \cos 4\varphi - \mu \text{ in polar coordinates, with } \varphi \text{ the azimuthal angle,} \\ a(k_x^2 + k_y^2) + (k_x^4 - 6k_x^2k_y^2 + k_y^4) - \mu \text{ in Cartesian coordinates} \end{cases} \quad (1)$$

For small non-zero positive a this dispersion exhibits two LTs as we sweep through the possible values of the chemical potential μ . At smaller values of μ one large hole-like Fermi surface exists. At the critical chemical potential four vHs appear at a topological transition of the Fermi surface where a new center pocket is created. As the chemical potential is increased further, the Fermi surface undergoes a second LT, of the band edge type, with the vanishing of the centre pocket. For $\text{Sr}_3\text{Ru}_2\text{O}_7$ these two topological transitions are nearly degenerate: they both happen almost at the same point in momentum space and chemical potential, justifying the treatment as a multicritical Lifshitz transition. If the system is tuned to $a = 0$, by e.g. uniform pressure, the vHs would merge with the minimum of the central electron pocket to form a 4th order saddle.

$$4 \times \underbrace{(k_x^2 - k_y^2)}_{\text{vH saddle}} + 1 \times \underbrace{k^2}_{\text{e/h pocket}} \longleftrightarrow \underbrace{k^4 \cos 4\varphi}_{\text{4th order saddle}} , \quad (2)$$

The singularity can be viewed as a Lifshitz multicritical point, as it appears at the crossing of two LTs and sits at the border of four different topological phases, see Fig. 3. Such behavior can be described within the framework of singularity theory²¹, by a symmetry-restricted unimodal parabolic singularity X_9 in the electron dispersion $\varepsilon(\vec{k})$. The core of the singularity is the 4th order terms, generalised to $k_x^4 + Kk_x^2k_y^2 + k_y^4$ in Cartesian coordinates. This term is the germ of the singularity, while the remaining terms $(a(k_x^2 + k_y^2) - \mu)$ represent the perturbation unfolding the singularity. Unlike simpler singularities, X_9 forms a whole family of singularities parametrized by the modulus K . While a generic singularity from the X_9 family has a co-dimension eight, one modulus and seven control parameters,

the presence of the lattice symmetry greatly simplifies the situation leaving only the modulus K and two control parameters a, μ . The consequences in physical properties of the singularity are the same for the whole range $K < -2$. In the case of $\text{Sr}_3\text{Ru}_2\text{O}_7$, the singularity is at the centre of the γ band and the DFT calculations suggest a value of K close to $K = -6$.

The DOS of states of this dispersion has a critical $\propto |\mu|^{-1/2}$ scaling for $a = 0$ and can be summarized as

$$\nu(\mu) \propto \begin{cases} |\mu - \mu_c|^{-1/2}, & |\mu| \gg \mu_c \\ \ln \frac{\mu_c}{|\mu - \mu_c|}, & |\mu - \mu_c| \ll \mu_c, \end{cases} \quad (3)$$

where the critical value of the chemical potential $\mu_c = a|a|/4$ (more details in the SI).

Magnetic Field Approach to Criticality. The multicritical LT has a profound effect on the specific heat as a function of the magnetic field ($C_v \propto |H - H_c|^{-1}$). The power law divergence of the DOS as a function of energy leads to the divergence of specific with the field¹². The heat capacity is determined by the value $nu(\epsilon_F)$ of the DOS at the Fermi energy: $C = \frac{\pi}{2} k_B T \nu(\epsilon_F)$. Near the singularity $\nu(\epsilon) \propto |\epsilon - \epsilon_c|^{-1/2}$, where ϵ_c is the location of the singularity. Including magnetic field to lowest order, the DOS becomes $\nu(\epsilon, H) = \frac{1}{2} (\nu(\epsilon + g\mu_B H) + \nu(\epsilon - g\mu_B H))$. Charge conservation requires the Fermi energy to shift non-linearly with H :

$$\sqrt{\epsilon_F(H) - \epsilon_c + g\mu_B H} + \sqrt{\epsilon_F(H) - \epsilon_c - g\mu_B H} = 2\sqrt{\epsilon_F(0) - \epsilon_c} \quad (4)$$

At H_c , $\epsilon_F(H_c) = \epsilon_c + g\mu_B H_c$ as the singularity is within the minority band. Then $\epsilon_F(0) - \epsilon_c = \frac{1}{2} g\mu_B H_c$ and for H near H_c Eq.(4) reads $\epsilon_F(H) = \epsilon_c + g\mu_B \frac{H^2 + H_c^2}{2H_c}$. As a consequence, $\nu(\epsilon_F(H)) \propto 1/|H - H_c|$ and the specific heat as well as the entropy is proportional to $1/|H - H_c|$, in agreement with the data. This is a direct fingerprint of the multicritical FS topological transition.

Phase Formation. As pointed out, there is significant nesting along \vec{Q}^A in the γ band giving rise to a susceptibility to SDW formation in addition to the metamagnetism originating from the multicritical LT. As the origin of the two transitions comes from different orbitally orthogonal parts of the Fermi surface, at tree-level in a Renormalization Group theory sense the two processes can be treated as decoupled. At higher order of RG this is no longer true and a positive feedback mechanism boosts the thermodynamic stability of the density wave via the DOS singularity. The mechanism of this particular Lifshitz transition as described above, involved the creation of a pocket in the middle of the γ band. A consequence of interaction effects, is that this formation is a first order transition, which involves a jump to a higher total number number of fermions²². As a result, the entropy jumps to a higher value at H_c when entering the A-phase, reflecting that change. The metamagnetic transition also is of first order as the free energy acquires non-analytic terms. For example, at $T = 0$ and for the DOS corresponding to $a = 0$ for simplicity, we find a term in the free energy proportional to $|\delta m|^{5/2}$ where δm is the jump in magnetisation. For completeness, in the SI we present, using scaling theory², the part of the free energy also due to the SDW formation, with an entropy that is logarithmically divergent at H_c . A more detailed treatment that couples the two phenomena is beyond the scope of the present work.

Temperature Approach to Criticality The third thermodynamic feature is the logarithmic divergence $C_v \propto T \log(1/T)$ (Fig. 1d). This is clearly an effect of interactions and a signature of quantum criticality. As shown by

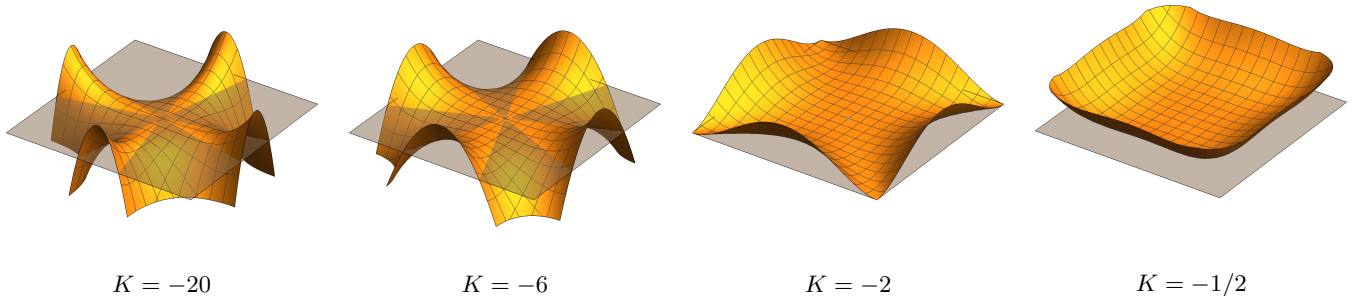


Figure 4: *Left:* The three dimensional surfaces above are electron dispersions $\epsilon = \epsilon(k_x, k_y)$ in the vicinity of the singularity. The grey horizontal plane represents the critical energy of the singularity $\epsilon = 0$. All values of the modulus $K < -2$ lead to the same topological features. The value of the modulus $K = -6$ corresponds to electron-like and hole-like sections of the same width, a property that is confirmed in the DFT calculation. This implies existence of an additional symmetry in the system, a superposition of the particle-hole transformation $\epsilon \leftrightarrow -\epsilon$ and rotation by an angle $\pi/4$. If we increase the value of the modulus, at $K = -2$ the system reaches a critical point and the saddle disappears leaving a singular $\propto k^4$ electronic pocket.

one of us in a previous work²⁵, the formation of a small pocket in the middle of a larger FS leads to the same result due to interactions. Similarly it can be thought as a consequence of the scattering of "light" electrons further from the singularity, off "heavy" electrons²⁴. It is also worth noting that a correlated 2D system with self-energy which is position-dependent (k -dependent) will lead to such behavior^{26,27}. In the case of SDW formation, the self-energy correction is $\Sigma(\omega, \vec{k}) \propto \omega/k$ (with $k = k_{||}$), giving an effective mass $m^* = m[1 - \partial\Sigma/\partial\omega|_{\omega \rightarrow 0}]$. As a consequence $C_v \propto T \int m^* dk$ leads to $C_v \propto T \log(1/T)$. Both conditions are fundamentally linked to the multicritical Lifshitz transition giving rise to qualitatively similar behaviour.

Discussion. In this work, we have demonstrated how a multicritical LT happening at a high symmetry point in the Brillouin zone can lead to rich physical phenomena. We illustrated this with $\text{Sr}_3\text{Ru}_2\text{O}_7$, in which a multicritical LT happens in the γ bands at the X-point of the Brillouin zone resulting in a 4-leaf ($n = 4$) Fermi surface. This is accompanied by a large peak in the DOS, which at relevant energies is describable by a square-root inverse singularity approaching the critical energy. We showed how this power-law in combination with the emergent central pocket and enhanced spin-/charge-susceptibilities due to independent, orbitally orthogonal parts of the Fermi surface are consistent with a wide range of previously puzzling experimental data including (i) singular contributions to C/T approaching H_C , (ii) the formation of the SDW close to the metamagnetic QCEP and (iii) entropy changes associated with entering the A-phase from low field.

We note that, although the singularity dominates the thermodynamics, the electrons there contribute indirectly, through the scattering of electrons from other parts of the FS off them, to the transport properties as the fermions are heavy (their Fermi velocity is almost zero) near the singular point. Therefore, there is a subtle interplay of the importance of each part of the Fermi surface to different experiments. Furthermore, the transition from the A-phase to B-phase, which has not been considered in this work, is most probably due to interaction effects and the renormalisation of the nested vector due to quantum fluctuations.

Finally we note that we only partially discuss those parts of the phase diagram of $\text{Sr}_3\text{Ru}_2\text{O}_7$ where quantum fluctuations contribute significantly. These dominate the details of transitions as a function of temperature (e.g. SDW), contribute to the $T \log(1/T)$ behavior of the specific heat and significantly renormalise the band structure as evidenced by the large Wilson ratio. The achievement of this work is to identify the importance of the multicritical topological FS transition and thereby help to disentangle the roles of the LT in the band structure on the one hand and (quantum) fluctuations and interactions on the other.

Finally we stress that multicritical LTs generically occur at points of high symmetry in the Brillouin zone. $\text{Sr}_3\text{Ru}_2\text{O}_7$ should not be seen as peculiar but a model system and guide to a whole range of material classes in which multicritical topological LT transitions occur (see supplementary information). One of the key lessons is that the associated non-trivial divergences in the DOS are a key driver in thermodynamically stabilising density waves originating from otherwise independent (orbitally orthogonal) parts of the Fermi surface.

Methods.

Our calculations were carried out within the local (spin) density approximation [L(S)DA] using the Full Potential Local Orbital band-structure package (FPLO)^{28,29} based on structural data published in³⁰. A mesh of $24 \times 24 \times 24$ k-points in the whole Brillouin zone was employed. Due to the rather sizable spin-orbit interaction of the Ru atoms, the full relativistic four-component Dirac scheme was used. To test the generality of the results, we used two different functionals, local density approximation (LDA) and generalized gradient approximation (GGA). The results are extremely similar for LDA and GGA, especially close to the Fermi energy.

Acknowledgements. We acknowledge helpful discussions with Andrey Chubukov, Felix Baumberger, Clifford Hicks. The work was supported by the EPSRC grant No. EP/P002811/1 and Royal Society (JJB) and DOE Grant No. DE-FG02-06ER46316 (CC).

¹ P. Dai, J. Hu & E. Dagotto, Magnetism and its microscopic origin in iron-based high-temperature superconductors *Nat. Phys.* **8**, 709 (2012).

² P. Monceau, Electronic crystals: an experimental overview, *Adv. Phys.* **61**, 325 (2012).

³ A.M. Gabovich, A.I. Voitenko & M. Ausloos, Charge- and spin-density waves in existing superconductors: competition between Cooper pairing and Peierls or excitonic instabilities, *Phys. Rep.* **367**, 583 (2002).

⁴ E. P. Wohlfarth & P. Rhodes, Collective Electron Magnetism *Phil. Mag.* **7**, 1817 (1962).

⁵ A. Shtyk, G. Goldstein & C. Chamon, Electrons at the monkey saddle: A multicritical Lifshitz point, *Phys. Rev. B* **95**, 035137 (2017).

⁶ A.P. Mackenzie, J.A.N. Bruin, R.A. Borzi, A.W. Rost & S.A. Grigera, Quantum criticality and the formation of a putative electronic liquid crystal in $\text{Sr}_3\text{Ru}_2\text{O}_7$, *Physica C* **481**, 207 (2012).

⁷ S. A. Grigera, P. Gegenwart, R. A. Borzi, F. Weickert, A. J. Schofield, R. S. Perry, T. Tayama, Sakakibara, Y. Maeno, A. G. Green & A. P. Mackenzie, Disorder-sensitive phase formation linked to metamagnetic quantum criticality, *Science* **306**, 1154 (2004).

⁸ S.-I. Ikeda, Y. Maeno, S. Nakatsuji., M. Kosaka & Y. Uwatoko Ground state in $\text{Sr}_3\text{Ru}_2\text{O}_7$ Fermi liquid close to a ferromagnetic instability. *Phys. Rev. B* **62**, R6089 (2000).

⁹ H. Yaguchi, R.S. Perry & Y. Maeno, Ferromagnetism induced by uniaxial pressure in the itinerant metamagnet $\text{Sr}_3\text{Ru}_2\text{O}_7$, *J. Low Temp. Phys.* **850**, 1203 (2006).

¹⁰ R. S. Perry, L. M. Galvin, S. A. Grigera, L. Capogna, A. J. Schofield, A. P. Mackenzie, M. Chiao, S. R. Julian, S. I. Ikeda, S. Nakatsuji, Y. Maeno, & C. Pfleiderer, Metamagnetism and critical fluctuations in high quality single crystals of the bilayer ruthenate $\text{Sr}_3\text{Ru}_2\text{O}_7$, *Phys. Rev. Lett.* **86**, 2661-2664 (2001).

¹¹ S.A. Grigera, R.S. Perry, A.J. Schofield, M. Chiao, S.R. Julian, G.G. Lonzarich, S.I. Ikeda, Y. Maeno, A.J. Millis, A.P. Mackenzie, Magnetic field-tuned quantum criticality in the metallic ruthenate $\text{Sr}_3\text{Ru}_2\text{O}_7$, *Science* **294**, 329 (2001).

¹² A. W. Rost, R. S. Perry, J. F. Mercure, A. P. Mackenzie, & S. A. Grigera, Entropy landscape of phase formation associated with quantum criticality in $\text{Sr}_3\text{Ru}_2\text{O}_7$, *Science* **325**, 1360 (2009).

¹³ Y. Tokiwa, M. McHalwat, R. S. Perry & P. Gegenwart, *Phys. Rev. Lett.* **116**, 226402 (2016).

¹⁴ D. Sun, A. W. Rost, R. S. Perry, A. P. Mackenzie & M. Brando, Low temperature thermodynamic investigation of the phase diagram of $\text{Sr}_3\text{Ru}_2\text{O}_7$ *Phys. Rev. B* **97**, 115101 (2018).

¹⁵ R. A. Borzi, S. A. Grigera, J. Farrell, R. S. Perry, S. J. S. Lister, S. L. Lee, D. A. Tennant, Y. Maeno, & A. P. Mackenzie, Formation of a nematic fluid at high fields in $\text{Sr}_3\text{Ru}_2\text{O}_7$, *Science* **315**, 214 (2007).

¹⁶ C. Lester, S. Ramos, R. S. Perry, T. P. Croft, R. I. Bewley, T. Guidi, P. Manuel, D. D. Khalyavin, E. M. Forgan & S. M. Hayden, *Nat. Mater.* **14**, 373 (2015).

¹⁷ J.F. Mercure, A.W. Rost, E.C.T. Farrell, S.W. Goh, R.S. Perry, M.L. Sutherland, S.A. Grigera, R.A. Borzi, P. Gegenwart, A.S. Gibbs & A.P. Mackenzie, Quantum oscillations near the metamagnetic transition in $\text{Sr}_3\text{Ru}_2\text{O}_7$, *Phys. Rev. B* **81**, 235103 (2010).

¹⁸ A. Tamai, M.P. Allan, J.-F. Mercure, W. Meevasana, R. Dunkel, D.H. Lu, R.S. Perry, A.P. Mackenzie, D.J. Singh, Z.-X. Shen & F. Baumberger, Fermi surface and van Hove singularities in the itinerant metamagnet $\text{Sr}_3\text{Ru}_2\text{O}_7$, *Phys. Rev. Lett.* **101**, 026407 (2008).

¹⁹ J. Lee, M.P. Allan, M.A. Wang, J. Farrell, S.A. Grigera, F. Baumberger, J.C. Davis & A.P. Mackenzie, Heavy d-electron quasiparticle interference and real-space electronic structure of $\text{Sr}_3\text{Ru}_2\text{O}_7$, *Nat. Phys.* **5**, 800 (2009).

²⁰ C. M. Puetter, J. G. Rau & H.-Y. Kee, Microscopic route to nematicity in $\text{Sr}_3\text{Ru}_2\text{O}_7$, *Phys. Rev. B* **81**, 081105(R) (2010).

²¹ V. I. Arnold, Singularity Theory, London Mathematical Society Lecture Note Series 53, Cambridge University press (1981).

²² S. Slizovskiy, J. J. Betouras, S. T. Carr & J. Quintanilla, Effect of paramagnetic fluctuations on a Fermi-surface topological transition in two dimensions, *Phys. Rev. B* **90**, 165110 (2014).

²³ L. Zhu, M. Garst, A. Rosch & Q. Si Universally diverging Gruneisen parameter and the magnetocaloric effect close to quantum critical points, *Phys. Rev. Lett.* **91**, 066404 (2003).

²⁴ E. Berg, S. Hartnoll & C. H. Mousatov, Theory of strange metals from hot electrons, to appear (2018).

²⁵ S. Slizovskiy, A. V. Chubukov & J. J. Betouras, Magnetic fluctuations and specific heat in Na_xCoO_2 near a Lifshitz transition, *Phys. Rev. Lett.* **114**, 066403 (2015).

²⁶ Sean A. Hartnoll, Diego M. Hofman, Max A. Metlitski & Subir Sachdev, Quantum critical response at the onset of spin-density-wave order in two-dimensional metals, *Phys. Rev. B* **84**, 125115 (2011).

²⁷ Ar. Abanov, A. V. Chubukov & J. Schmalian, Quantum-critical theory of the spin-fermion model and its application to cuprates: Normal state analysis, *Adv. Phys.* **52**, 119 (2003).

²⁸ K. Koepernik & H. Eschrig, Full-potential nonorthogonal local-orbital minimum-basis band-structure scheme, *Phys. Rev. B* **59**, 1743 (1999).

²⁹ <http://www.fplo.de>.

³⁰ H. Shaked, J.D. Jorgensen, O. Chmaissem, S. Ikeda & Y. Maeno, Neutron Diffraction Study of the Structural Distortions in $\text{Sr}_3\text{Ru}_2\text{O}_7$, *Journal of Solid State Chemistry* **154**, 361 (2000).

SUPPLEMENTAL INFORMATION

I. DENSITY OF STATES IN THE VICINITY OF THE MULTICRITICAL POINT

As we discuss in the main text, the physics of the multicritical Lifshitz point can be described by the dispersion

$$\varepsilon(\vec{p}) = ap^2 + bp^4 \cos 4\varphi + cp^8 - \mu. \quad (\text{S1})$$

Below we assume small values of a and μ . In this case the p^8 term is not crucial for the analysis, as it only serves to close the Fermi surface away from the singularity, and it can be omitted safely,

$$\varepsilon(\vec{p}) \simeq ap^2 + bp^4 \cos 4\varphi - \mu. \quad (\text{S2})$$

For definiteness we assume $a > 0$ below. The symmetry of the dispersion Eq. (S2) implies the relation $\nu(-|a|, \mu) = \nu(|a|, -\mu)$. The DoS of (S2) is given by

$$\nu(\mu) = \int \frac{d^2 p}{(2\pi)^2} \delta(ap^2 + bp^4 \cos 4\varphi - \mu) = \int \frac{d\varphi dt}{8\pi^2} \delta(at + bt^2 \cos 4\varphi - \mu) = \frac{1}{4\pi^2 a} D\left(\frac{4b\mu}{a^2}\right), \quad (\text{S3})$$

where we made a substitution $t = p^2$ and the function $D(x)$ is an elliptic integral

$$D(x) = \int_0^{2\pi} d\varphi \int_0^\infty dt \delta(2t + t^2 \cos \varphi - x) = 2\Re \int_0^\infty dt \frac{1}{\sqrt{t^4 - (2t - x)^2}}. \quad (\text{S4})$$

The DoS obtained above has a natural energy scale

$$\mu_c = a^2/4b. \quad (\text{S5})$$

A. Critical scaling at $|\mu| \gg \mu_c$

The term ap^2 breaks the multicriticality, so that at large values of the chemical potential $|\mu| \gg a^2/4b$, when quadratic term can be neglected, the dispersion reduces to the pure fourth-order saddle

$$\varepsilon(\vec{p}) = bp^4 \cos 4\varphi - \mu \quad (\text{S6})$$

with the critical scaling of the DoS $\nu(\mu) \propto |\mu|^{-1/2}$,

$$\nu(\mu) = \int \frac{d^2 p}{(2\pi)^2} \delta(bp^4 \cos 4\varphi - \mu) = \frac{1}{4\pi^2 \sqrt{b|\mu|}} \int d^2 k \delta(k^4 \cos 4\varphi - 1) = \frac{K(1/2)}{4\sqrt{2}\pi^2} \frac{1}{\sqrt{b|\mu|}} \propto |\mu|^{-1/2}, \quad (\text{S7})$$

where $K(1/\sqrt{2}) \approx 1.85$ is a complete elliptic integral of the first kind.

B. Jump at $\mu = 0$

As we approach the singularity from the region of negative chemical potential, the quadratic term leads to the formation of electron pocket at the center. The electron pocket forms at $\mu = 0$ and leads to a jump in the density of states,

$$\begin{aligned} \nu(\mu = +0) - \nu(\mu = -0) &= \lim_{\mu \rightarrow +0} \int \frac{d^2 p}{(2\pi)^2} \delta(ap^2 + bp^4 \cos 4\varphi - \mu) - \lim_{\mu \rightarrow -0} \int \frac{d^2 p}{(2\pi)^2} \delta(ap^2 + bp^4 \cos 4\varphi - \mu) \\ &= \lim_{\mu \rightarrow +0} \int \frac{d^2 p}{(2\pi)^2} \delta(ap^2 - \mu) = \frac{1}{4\pi a}. \end{aligned} \quad (\text{S8})$$

C. Van Hove singularity at $\mu = \mu_c$

Finally, at the value of the chemical potential $\mu = \mu_c = a^2/4b$ the electron pocket formed at $\mu = 0$ touches four outer leaves of the Fermi surface via the formation of four saddle points, located at $p_c = \sqrt{a/2b}$, $\cos 4\varphi_c = -1$:

$$\begin{aligned} ap^2 + bp^4 \cos 4\varphi - \mu &\approx a(p_c + \Delta p)^2 - b(p_c + \Delta p)^4 \left(1 - \frac{(4\Delta\varphi)^2}{2}\right) - \mu \\ &= (ap_c^2 - bp_c^4 - \mu) + (2ap_c - 4bp_c^3)\Delta p + (a - 6bp_c^2)(\Delta p)^2 + 8bp_c^4(\Delta\varphi)^2 \\ &= (\mu - \mu_c) - 2a(\Delta p)^2 + 8\mu_c(\Delta\varphi)^2. \end{aligned} \quad (\text{S9})$$

The saddle point result in the logarithmic divergence in the DoS:

$$\begin{aligned} \nu(\mu) &= 4 \int \frac{d^2p}{(2\pi)^2} \delta((\mu - \mu_c) - 2a(\Delta p)^2 + 8\mu_c(\Delta\varphi)^2) \\ &= \frac{1}{2\sqrt{2}\pi^2 a} \int dx dy \delta\left(\frac{\mu - \mu_c}{\mu_c} - x^2 + y^2\right) \\ &\simeq \frac{1}{\sqrt{2}\pi^2 a} \log \frac{\mu_c}{|\mu - \mu_c|}. \end{aligned} \quad (\text{S10})$$

These results can be confirmed by studying limits of the general expression (S3).

D. General expression (S3)

Using a substitution $z = (t - x)/t$ the elliptic integral $D(x)$ can be rewritten as

$$D(x) = 2\text{Re} \int_{-sgn(x)}^{\infty} \frac{dz}{\sqrt{[(|x| - 1) + z^2][(|x| + 1) - z^2]}}. \quad (\text{S11})$$

Taking the real part of the integral above just reduces the integration to the region where the argument of the square root is positive. Depending on the value of x , the true domain of integration is

$$\begin{aligned} x > 1 : \quad z &\in (-1, \sqrt{1 + |x|}), \\ 0 < x < 1 : \quad z &\in (-1, -\sqrt{1 - |x|}) \cup (\sqrt{1 - |x|}, \sqrt{1 + |x|}), \\ x < 0 : \quad z &\in (1, \sqrt{1 + |x|}). \end{aligned} \quad (\text{S12})$$

Transforming the variable as $z = \sqrt{(|x| + 1)} \cos \theta$ we bring the integral to the canonical form

$$D(x) = \sqrt{\frac{2}{|x|}} \times \begin{cases} F(\pi - \varphi_1(x), k(x)), & x > 1 \\ 2F(\varphi_2(x), k(x)) - F(\varphi_1(x), k(x)) & 0 < x < 1 \\ F(\varphi_1(x), k(x)), & x < 0 \end{cases} \quad (\text{S13})$$

where modulus and angles are

$$k(x) = \sqrt{\frac{1 + |x|}{2|x|}}, \quad \varphi_1 = \arctan(\sqrt{|x|}), \quad \varphi_2 = \arctan \sqrt{\frac{2|x|}{1 - |x|}}. \quad (\text{S14})$$

At large values of the argument the asymptotic behavior is

$$D(x) \simeq \sqrt{\frac{2}{|x|}} K\left(\frac{1}{\sqrt{2}}\right), \quad |x| \gg 1, \quad (\text{S15})$$

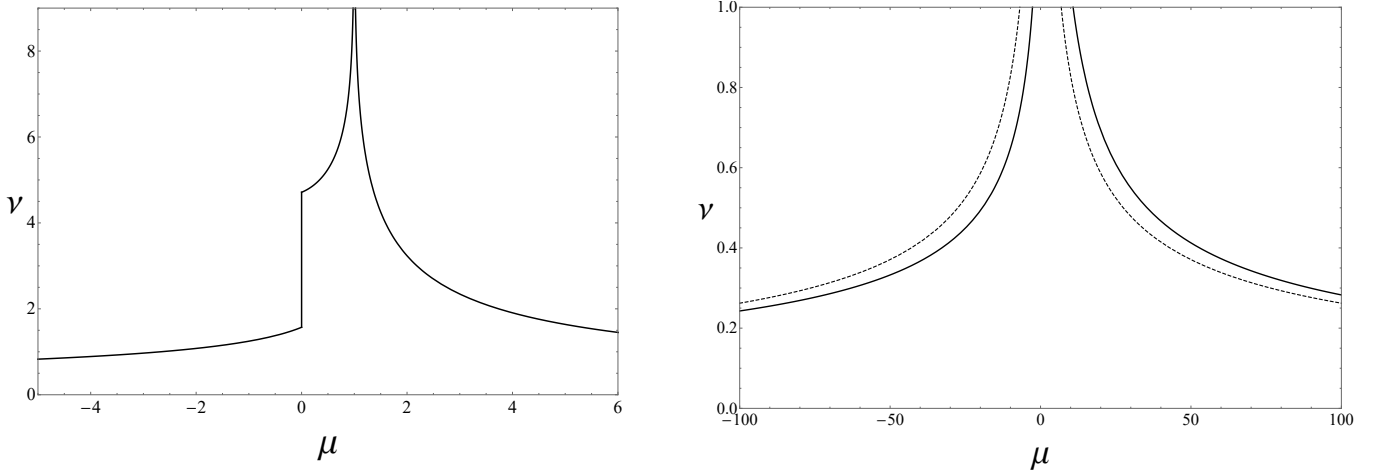


Figure S1: DoS $\nu(\mu) \equiv D(\mu)$, with DoS and chemical potential in units $(4\pi^2a)^{-1}$ and $\mu_c = a^2/4b$ respectively. The plot on the right shows DoS at larger values of the chemical potential when the singularity breaking term ap^2 can be neglected. The dashed line shows the critical scaling of the DoS given by (S15), $\nu(\mu) \propto |\mu|^{-1/2}$.

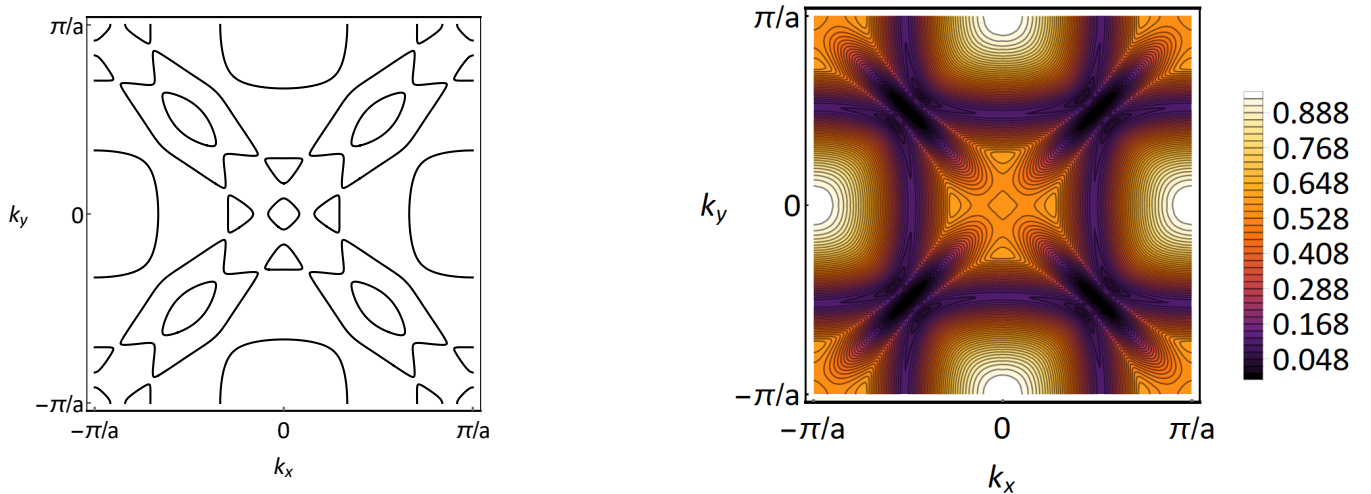


Figure S2: Fermi surface (left) and energy dispersion of the 4th band (right). Momentum is centered around γ bands, where the Lifshitz multipoint resides. However, for given Hamiltonian parameters it is decomposed into four van Hove saddles

II. EFFECTIVE HAMILTONIAN

In the main text we showed the presence of multicritical Lifshitz point in $\text{Sr}_3\text{Ru}_2\text{O}_7$ via DFT calculation. Here, we show that it is also present within a tight-binding model as presented in Ref. S1, which reads:

$$H = \sum_{\vec{k}, \alpha} \Psi_{\vec{k}\alpha}^\dagger \begin{pmatrix} A_{\vec{k}} & G \\ G^* & A_{\vec{k}+\vec{Q}} \end{pmatrix} \Psi_{\vec{k}\alpha}, \quad (\text{S16})$$

where $\alpha = \uparrow\downarrow$ is a spin index, $\vec{Q} = (\pi/a, \pi/a)$ and

$$A_{\vec{k}} = \begin{pmatrix} \varepsilon_{\vec{k}}^{yz} & \varepsilon_{\vec{k}}^{1D} + i\lambda & -\lambda \\ \varepsilon_{\vec{k}}^{1D} - i\lambda & \varepsilon_{\vec{k}}^{xz} & i\lambda \\ -\lambda & i\lambda & \varepsilon_{\vec{k}}^{xy} \end{pmatrix}, \quad G = \begin{pmatrix} \bar{g} & 0 & 0 \\ 0 & \bar{g} & 0 \\ 0 & 0 & \bar{g} \end{pmatrix}. \quad (\text{S17})$$

The matrix A describes the hopping between three yz, xz, xy orbitals with spin-orbital coupling λ included. The dispersions of three individual orbitals are

$$\begin{aligned}\varepsilon_{\vec{k}}^{yz} &= -2t_1 \cos(k_y a) - 2t_2 \cos(k_z a), \\ \varepsilon_{\vec{k}}^{xz} &= -2t_1 \cos(k_x a) - 2t_2 \cos(k_z a), \\ \varepsilon_{\vec{k}}^{xy} &= -2t_3(\cos(k_x a) + \cos(k_y a)),\end{aligned}\quad (\text{S18})$$

while $\varepsilon_{\vec{k}}^{1D} = -4t_6 \sin(k_x a) \sin(k_y a)$ describes the hopping between two quasi-one-dimensional orbitals yz and xz . The matrix G describes unit-cell doubling via an effective lattice potential. The parameters of the Hamiltonian are

$$t_1 = 0.5, t_2 = 0.05, t_3 = 0.5, t_4 = 0.1, t_5 = -0.03, t_6 = 0.05, \lambda = 0.1375, \bar{g} = 0.1. \quad (\text{S19})$$

The chemical potential can be determined self-consistently via the DoS that follows from (S18) and is $\mu = 0.575$. Fermi surface is shown in the Fig. S2 (left), which is centered around γ bands. For given parameters Hamiltonian is only in the vicinity of the topological multiple point and the singularity is decomposed into four van Hove saddles.

Finally, even in this simple model there is a nesting between the parts of the γ bands, that leads to the formation of the spin density wave. Examining eigenvalues of the Hamiltonian, we find that it is the 4th band that is involved in the formation of the multiple point around the Fermi energy. Given the C_4 rotational symmetry of the system, to show the presence of nesting, it is enough to calculate the curvature of this 4th band,

$$\kappa(k_x, k_y) = \frac{2E_x E_y E_{xy} - E_x^2 E_{yy} - E_y^2 E_{xx}}{(E_x^2 + E_y^2)^{3/2}} \quad (\text{S20})$$

where $E \equiv E(k_x, k_y)$ is the dispersion of the 4th band and $E_i \equiv \partial E / \partial k_i$ and $E_{ij} \equiv \partial^2 E / \partial k_i \partial k_j$ are partial derivatives. Using symmetry arguments again, it is enough to find whether the following condition can be satisfied:

$$\kappa\left(\frac{\vec{Q}}{2}, 0\right) \propto \frac{\partial^2 E}{\partial k_y^2}\left(\frac{\vec{Q}}{2}, 0\right) = 0. \quad (\text{S21})$$

We calculate numerically the second derivative E_{yy} of the electron dispersion of the 4th band and show that it turns to zero at the nesting vector $\vec{Q} = (\pm 0.29, 0, 0)(2\pi/a)$ (See Fig. S3). In this way we confirm the presence of the nesting in the system. The value we find is slightly different from the experimental finding of $\vec{Q}_{\text{exp}} = (\pm 0.233, 0, 0)(2\pi/a)$. It is important to stress that

- it is a simple tight-binding model without interactions.
- there is no fine-tuning of the effective Hamiltonian, as exactly the same parameters as in Ref. S1 has been used.

As a result, here we confirm the presence of the nesting using the tight binding Hamiltonian, while the actual quantitative features are reproduced with the *ab initio* approach of LDA calculation presented in the main text.

III. ENTROPY NEAR H_c FOR A SDW INSTABILITY

According to scaling theory, for the SDW transition^{S2}, if the critical part of the free energy is separated, then $\mathcal{F}_{\text{crit}}^{\text{SDW}} = -\rho_0 \left(\frac{T}{T_0}\right)^{\frac{d+z}{z}} f((H - H_c)/(T/T_0)^{\frac{1}{\nu z}}) + \text{logarithmic corrections as } \frac{T_0(H - H_c)}{TH_c} \rightarrow 0$. T_0 and ρ_0 and c are non-universal constants, $d = 2$ is the dimensionality of the system, $z = 2$ the dynamical exponent, $\nu = 1/2$ the exponent that shows the divergence of the coherence length ξ close to the transition $\xi \propto |\frac{H - H_c}{H_c}|^{-\nu}$ and $f(x)$ is a regular function, which can be expanded close to $x = 0$. Therefore in the limit $\frac{T_0(H - H_c)}{TH_c} \rightarrow 0$

$$\mathcal{F}_{\text{crit}}^{\text{SDW}} = -\rho_0 \left[\left(\frac{T}{T_0}\right)^2 f(0) + \frac{H - H_c}{H_c} \frac{T_0}{T} f'(0) + \text{clog} \left(\frac{H_c}{|H - H_c|} \right) \right] \quad (\text{S22})$$

leading to an increase in entropy close to H_c due to the logarithmic divergence.

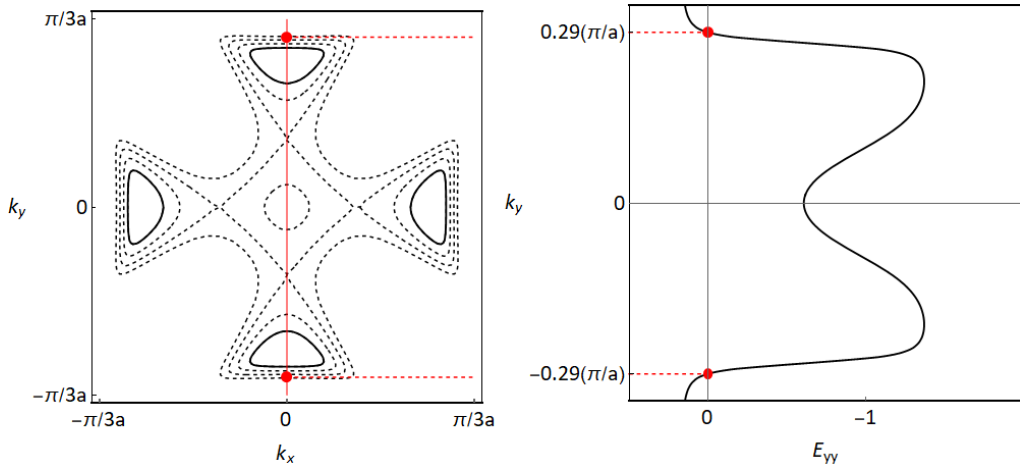


Figure S3: Surfaces (left) of constant energy for the 4th band and the second derivative E_{yy} along the y -axis (right). The second derivative E_{yy} turns to zero at $\vec{Q}/2 = (0.29, 0, 0)(\pi/a)$ indicating a flat Fermi surface at this energy and the presence of the nesting.

IV. HIGHER ORDER SINGULARITIES IN OTHER MATERIALS

The pivotal concept introduced in the main text controlling the wealth of phenomena observed in $\text{Sr}_3\text{Ru}_2\text{O}_7$ is the existence of a multi-critical Lifshitz point interacting with an incipient nesting feature. Naturally a key question is the generality of this concept and its suitability as a guiding principle in material design.

The aim of this section is to show that there are indeed generic mechanisms generating such multicritical Lifshitz points in a wide range of material classes making them an extremely valuable 'material design guide'. A detailed analysis of all materials discussed here along the lines of the one presented for $\text{Sr}_3\text{Ru}_2\text{O}_7$ would certainly go beyond the scope of this paper. However, we believe that the existence of multicritical Lifshitz points in the material classes identified below play an important role in the boosting and stabilising the observed physical phenomena and should be taken into consideration in the analysis of effective low energy hamiltonians of these systems.

A. Direct generalisation of $\text{Sr}_3\text{Ru}_2\text{O}_7$

In order to appreciate the generality of the multicritical Lifshitz point in $\text{Sr}_3\text{Ru}_2\text{O}_7$ it is instructive to scrutinize the details of a low energy tight binding model based on the relevant Ru 4d orbitals. In figure S6a we show the DFT band structure calculation described in the main text along the relevant high symmetry directions in the $k_z = 0$ plane of the 3D Brillouin zone of this quasi-2D material. In red we emphasise the part of the band structure giving rise to the multicritical Lifshitz point. Following previous work^{S3-S6} we developed an effective 2D tight binding model of a bilayer of RuO octahedra constrained to the relevant Ru 4d orbitals. In figure S6b we show the dispersion of this tight binding model along the equivalent high symmetry directions of figure S6a with an overall good agreement.

In this energy regime the orbital character of the band structure is predominantly that of the t_{2g} submanifold containing d_{xy} , d_{yz} and d_{zx} orbitals. One of the advantages of the tight binding model is the possibility of selectively removing orbitals and / or in order to study the impact on the relevant band structure features. In figure S6c we have for example removed the d_{yz} and d_{zx} orbitals. As can be seen this effectively leaves the dispersion giving rise to the multicritical Lifshitz point unchanged. This of course is equivalent to the observation that in the DFT calculation the relevant part of the band structure has effectively no $4d_{yz/zx}$ character and is predominantly d_{xy} with a small contribution of the e_g orbitals^{S6}.

At this point it is important to briefly discuss in how far the DFT band structure is relevant to the experimentally observed band structure of this strongly correlated material. Direct observation of the Fermi surface and the determination of effective masses and Fermi velocities has been achieved by ARPES^{S8,S9}, STM^{S10} and quantum oscillation^{S11} measurements. Crucially in particular the ARPES work has demonstrated that the band structure in the vicinity of the X-point is well described by an overall renormalised band structure and is qualitatively well described by LDA. We have verified that the tight binding model described below is fully consistent with the van Hove singularity observed in ARPES^{S8} confirming the arguments for generality presented here.

The two copies of the band structure apparent in S6c are the result of a bilayer split. Otherwise the tight binding model is that of a 2D square lattice with equivalent hopping along x and y axis including the following features:

1. A $\sqrt{2} \times \sqrt{2}$ reconstruction of the Brillouin zone. In the case of $\text{Sr}_3\text{Ru}_2\text{O}_7$ this is achieved by a counterrotation of neighbouring octahedra but could also be due to e.g. antiferromagnetic ordering or charge disproportionation or the momentum space picture of (π, π) charge-/spin-density-waves.
2. a small hybridisation gap opening at the zone boundary and in particular at the high-symmetry X point between the original and backfolded bands.

These ingredients are fully sufficient to generate the multicritical Lifshitz point. The resulting band structure (constrained by ARPES^{S8}) in the vicinity of the X -point retaining these minimal ingredients is shown in figure S5. In panel (a) we reproduce a schematic of the Fermi surface of $\text{Sr}_3\text{Ru}_2\text{O}_7$ for orientation (based on^{S11}). The multicritical Lifshitz point is located close to the X -point. In red we highlight the same parts of the band structure as in figure S6. The inset in the top-right corner shows the location and orientation of the contour plots shown in panel (b) and (c). In the former we present the tight binding model excluding the $4d_{yz/zx}$. The location of the Lifshitz points is indicated by the red crosses. Intriguingly the Fermi surface of this model does not produce the small closed pockets highlighted in panel (a). These are only recovered if the much more strongly dispersing bands originating from $4d_{yz/zx}$ are reintroduced as shown in panel (c)^{S24}. Remarkably it is the resulting flat parts that give rise to a nesting vector (blue) consistent with the spin density wave observed in neutron scattering^{S12}. It is this feature that drives the density wave phase within the theoretical model discussed in the main text. Within our model it is merely coincidence that the nested part of the band structure determining the density wave vector is part of the same Fermi surface giving rise to the multicritical Lifshitz point - these two components originate from completely separate, weakly hybridising bands with very different orbital character. From a material design point of view this is extremely important in that a multicritical Lifshitz point can boost / thermodynamically stabilise incipient order driven by otherwise unrelated parts of the Fermi surface.

As a side note we would like to remark that a fit of equation (3) in the main text to this low energy band structure results in K being of the order of -3 consistent with our analysis. Indeed it can be shown that a hamiltonian of form (B1) in ref.^{S13} will generally result in $K \leq -2$ as required for the validity of our theoretical analysis.

Irrespective of the detailed parameters for $\text{Sr}_3\text{Ru}_2\text{O}_7$ it is remarkable that such few ingredients are required for the stabilisation of the multicritical Lifshitz point for a tight binding model on a square lattice. Consequently one would expect these to be e.g. ubiquitous across the whole family of ruthenates. Indeed further examples in this family are:

Ruthenates - Surface layer of Sr_2RuO_4 The most straight forward realisation of a multicritical Lifshitz point as described above is occurring in the surface layer of Sr_2RuO_4 . All key ingredients exist: (i) a vHs at the M point of the ideal band structure, (ii) backfolding due to rotation of RuO_2 octahedra changing the C_2 symmetric singularity into a C_4 symmetric one at the X -point of the new surface Brillouin zone and finally (iii) hybridisation of the backfolded bands due to higher order hopping terms. Indeed ARPES measurements reveal a band structure consistent with this model located just 10meV below the Fermi energy^{S6}. It would be interesting to study the evolution of the surface electronic structure in spectroscopic studies under magnetic field by e.g. STM.

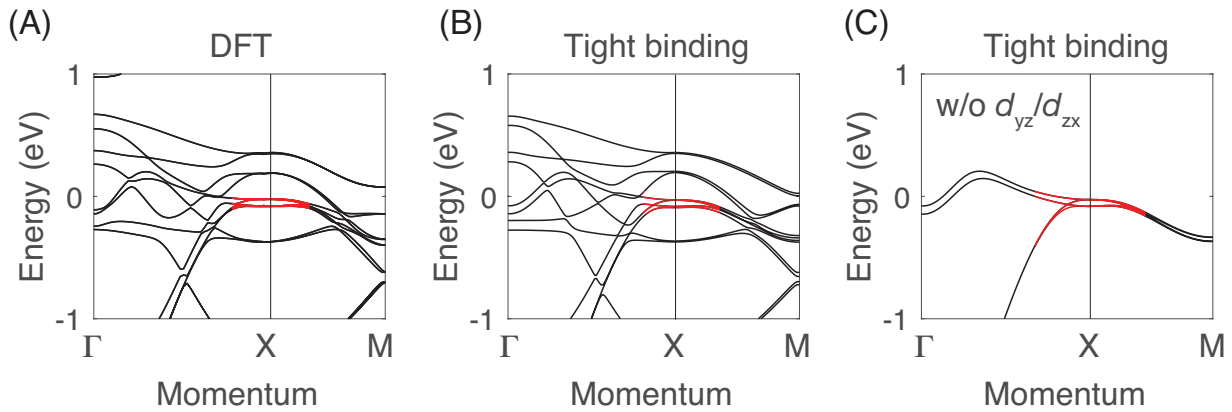


Figure S4: (a) Result of the DFT calculation along relevant high symmetry directions of the Brillouin zone. The part of the band structure giving rise to the multicritical Lifshitz point is emphasised in red. (b) Dispersion of an effective 2D tight binding model of a bilayer of RuO_2 octahedra based on Ru 4d orbitals. (c) Same tight binding model as in (b) but with the Ru $4d_{yz/zx}$ orbitals removed from the model.

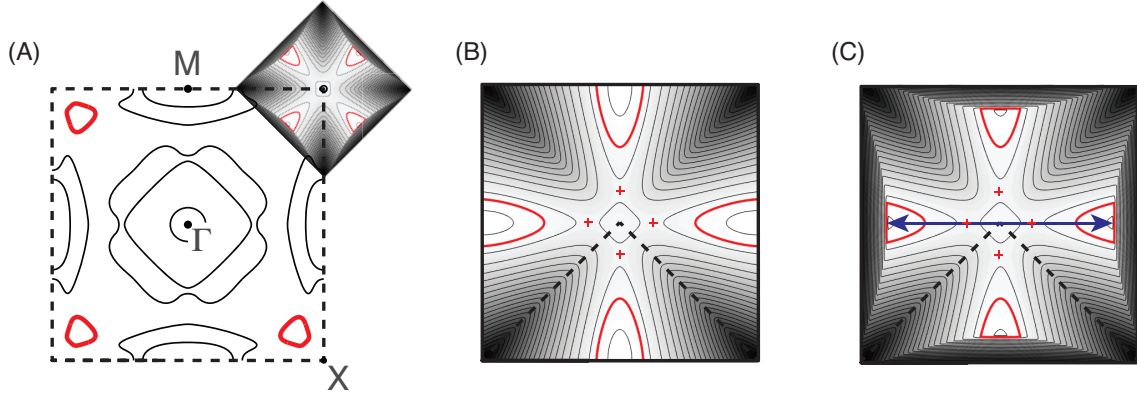


Figure S5: (a) Schematic of Fermi surface of $\text{Sr}_3\text{Ru}_2\text{O}_7$ (based on a figure in^{S11}). The red parts of the Fermi surface are those relevant to the multicritical Lifshitz point. They are generally referred to as γ_2 pockets in the literature. The overlay centred on the top right X-point is showing the location of the contour plots in the subsequent panels. (b) Contour plot of the minimal model generating multicritical Lifshitz points (red crosses). (c) Upon including the $d_{yz/zx}$ orbitals the γ_2 pockets are reproduced. This results in nested Fermi surface features (blue arrow) originating from different bands than the multicritical Lifshitz point (red cross).

Ruthenates - $\text{Ca}_3\text{Ru}_2\text{O}_7$ In the case of $\text{Ca}_3\text{Ru}_2\text{O}_7$ the relevant physics originates not from a d_{xy} band but from two $d_{xz/yz}$ bands with next nearest neighbour hopping^{S14}. An alternating c -axis tilt of the RuO octahedra then generates a backfolding of the band structure. At this point there is no singularity in the density of states at half filling. However, the combination of bilayer splitting and hybridisation generate singularities in the density of states located at the X-points of the Brillouin zone. Most interestingly this system subsequently undergoes a density wave order transition at app. 40 K^{S15}.

Cuprates The nature of charge- and spin-exitations as well as (short range) density wave formation in cuprates is of course a subject of ongoing discussions. However an often used starting point for theoretical calculations that is well motivated by experimental observations by ARPES and quantum oscillations is a band structure originating from the close-to-half filled d_{xy} band on a square lattice. This of course is exactly the situation as encountered in $\text{Sr}_3\text{Ru}_2\text{O}_7$. Consequently any $\sqrt{2} \times \sqrt{2}$ reconstruction of the unit cell (by e.g. (short range) magnetic order) in combination with a hybridisation gap opening between the original and back-folded bands will therefore generate exactly the same type of multicritical Lifshitz point as discussed for the example of $\text{Sr}_3\text{Ru}_2\text{O}_7$. This by no means is intended to be an explanation for the wealth of strong-coupling phenomena observed in cuprates but is merely to be seen as an exemplification of the generality of the concepts discussed in this paper and should potentially be taken carefully into account when discussing effective weak coupling hamiltonians.

B. Further materials

In this final section we would like to highlight the breadth of materials across many different 'families' in which multicritical Lifshitz points occur close or at the Fermi energy with potentially crucial impact on the stabilisation of incipient ordered phases. We would like to emphasise that neither is this an exhaustive list nor are we giving a review over the literature on these materials but merely intend to provide the interested reader with starting points to the extensive experimental literature.

BaFe_2As_2 -Iron based superconductors In figure S6a we show schematically the Fermi surface of BaFe_2As_2 based superconductors (see e.g.^{S16} for a more recent paper and citations therein). The typical 'clover leaf' structure of a Fermi surface close to a multicritical Lifshitz point can be clearly identified close to the X-Point. Recently it has been shown that this part of the band structure gives rise to a singular Fermi surface in the related compound $\text{SmFe}_{0.92}\text{Co}_{0.08}\text{AsO}$ ^{S16}.

Transition metal dichalcogenides - 1T-VSe₂ In figure S6b we show the evolution of the band structure with energy of a monolayer of the transition metal dichalcogenide VSe₂ recently studied by ARPES^{S17}. This is an example of an $n = 6$ multicritical Lifshitz point close to the Γ -point of the Brillouin zone. The singularity is located within 20 meV of the Fermi surface. Intriguingly a charge density wave order setting in at $T_C = 140$ K has been observed in the same study. Similar physics has been seen in the related 3D band structure / phase diagram of bulk VSe₂^{S18,S19}.

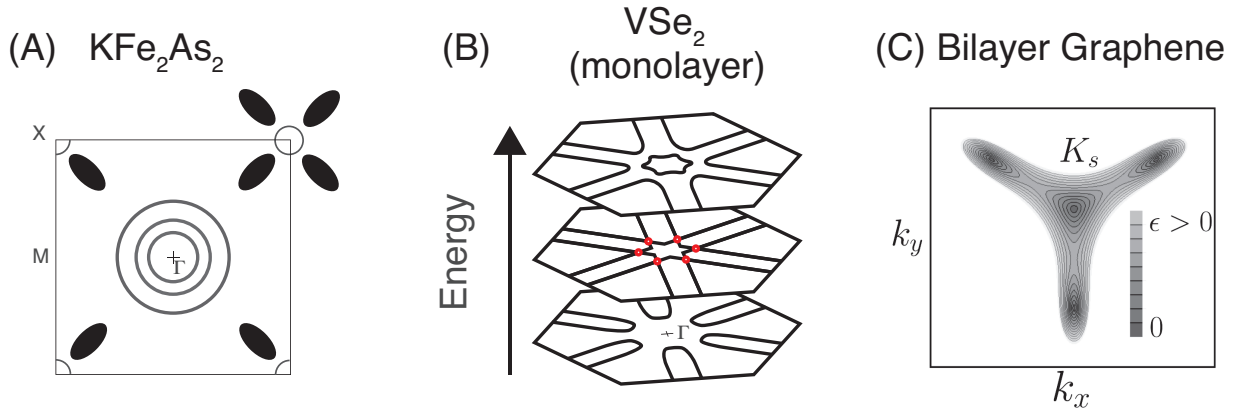


Figure S6: (a) Fermi surface of BaFe_2As_2 based iron based superconductors. in the top right corner we emphasise the typical 'glove leave' Fermi surface structure of incipient $n = 4$ multicritical Lifshitz points (see e.g.^{S16}). (b) Evolution of the band structure with energy of a monolayer of the transition metal dichalcogenide VSe_2 ^{S17}. The Lifshitz points are highlighted (red). (c) Contour plot of the $n = 3$ multicritical Lifshitz point (monkey saddle) in twisted bilayer graphene (reproduced from^{S21}).

and other transition metal dichalcogenides (see e.g. references in the introduction of^{S17}).

Twisted Bilayer Graphene Recently twisted bilayer graphene has come to the fore of condensed matter research by the experimental discovery of interaction driven insulating behaviour and the development of unconventional superconductivity^{S22,S23}. The band structure of these materials gives naturally rise to $n = 3$ multicritical points at the K/K' points of the 2D Brillouin zone (see figure S6b) and it can be shown that these play a potentially crucial role in the stabilisation of the observed electron-correlation driven phases^{S20,S21}.

[S1] C. M. Puetter, J. G. Rau, and H.-Y. Kee, Microscopic route to nematicity in $\text{Sr}_3\text{Ru}_2\text{O}_7$, *Phys. Rev. B* **81**, 081105(R) (2010).

[S2] L. Zhu, M. Garst, A. Rosch, and Q. Si Universally diverging Gruneisen parameter and the magnetocaloric effect close to quantum critical points. *Phys. Rev. Lett.* **91**, 066404 (2003).

[S3] M. H. Fischer and M. Sigrist, Effect of a staggered spin-orbit coupling on the occurrence of a nematic phase in $\text{Sr}_3\text{Ru}_2\text{O}_7$, *Phys. Rev. B* **81**, 064435 (2010)

[S4] C. Piefke F. Lechermann, LDA+ slave-boson approach to the correlated electronic structure of the metamagnetic bilayer ruthenate $\text{Sr}_3\text{Ru}_2\text{O}_7$, *Phys. Status Solidi B* **248**, 2269?2275 (2011)

[S5] C. Autieri, M. Cuoco and C. Noce, Structural and electronic properties of $\text{Sr}_2\text{RuO}_4/\text{Sr}_3\text{Ru}_2\text{O}_7$ heterostructures, *Phys. Rev. B* **89**, 075102 (2014)

[S6] E. Rozbicki, Effects of spin-orbit coupling and many-body interactions on the electronic structure of Sr_2RuO_4 , PhD Thesis, University of St Andrews (2011)

[S7] J.-F. Mercure, The de Haas van Alphen effect near a quantum critical end point in $\text{Sr}_3\text{Ru}_2\text{O}_7$, PhD Thesis, University of St Andrews (2008)

[S8] A. Tamai, M.P. Allan, J.-F. Mercure, W. Meevasana, R. Dunkel, D.H. Lu, R.S. Perry, A.P. Mackenzie, D.J. Singh, Z.-X. Shen, and F. Baumberger, Fermi surface and van Hove singularities in the itinerant metamagnet $\text{Sr}_3\text{Ru}_2\text{O}_7$, *Phys. Rev. Lett.* **101**, 026407 (2008)

[S9] M. P. Allan, A. Tamai, E. Rozbicki, M. H. Fischer, J. Voss, P. D. C. King, W. Meevasana, S. Thirupathaiah, E. Rienks, J. Fink, D. A. Tennant, R. S. Perry, J. F. Mercure, M. A. Wang, J. Lee, C. J. Fennie, E.-A. Kim, M. J. Lawler, K. M. Shen, A. P. Mackenzie, Z.-X. Shen and F. Baumberger, Formation of heavy d-electron quasiparticles in $\text{Sr}_3\text{Ru}_2\text{O}_7$, *New Journal of Physics* **15**, 063029 (2013)

[S10] J. Lee, M.P. Allan, M.A. Wang, J. Farrell, S.A. Grigera, F. Baumberger, J.C. Davis, and A.P. Mackenzie, Heavy d-electron quasiparticle interference and real-space electronic structure of $\text{Sr}_3\text{Ru}_2\text{O}_7$, *Nat. Phys.* **5**, 800 (2009)

[S11] J.F. Mercure, A.W. Rost, E.C.T. O'Farrell, S.W. Goh, R.S. Perry, M.L. Sutherland, S.A. Grigera, R.A. Borzi, P. Gegenwart, A.S. Gibbs, and A.P. Mackenzie, Quantum oscillations near the metamagnetic transition in $\text{Sr}_3\text{Ru}_2\text{O}_7$, *Phys. Rev. B* **81**, 235103 (2010)

[S12] C. Lester, S. Ramos, R. S. Perry, T. P. Croft, R. I. Bewley, T. Guidi, P. Manuel, D. D. Khalyavin, E. M. Forgan, and S. M. Hayden, *Nat. Mater.* **14**, 373 (2015)

[S13] A. M. Berridge, Role of band structure in the thermodynamic properties of itinerant metamagnets, *Phys. Rev. B* **83**, 235127 (2011)

- [S14] N. Kikugawa, A. W. Rost, C. W. Hicks, A. J. Schofield, and A. P. Mackenzie, $\text{Ca}_3\text{Ru}_2\text{O}_7$: Density Wave Formation and Quantum Oscillations in the Hall Resistivity, *Journal of the Physical Society of Japan* 79, 024704 (2010)
- [S15] F. Baumberger, N. J. C. Ingle, N. Kikugawa, M. A. Hossain, W. Meevasana, R. S. Perry, K. M. Shen, D. H. Lu, A. Damascelli, A. Rost, A. P. Mackenzie, Z. Hussain, and Z.-X. Shen, Nested Fermi Surface and Electronic Instability in $\text{Ca}_3\text{Ru}_2\text{O}_7$, *PRL* 96, 107601 (2006)
- [S16] A. Charnukha, S. Thirupathaiah, V. B. Zabolotnyy, B. Bchner, N. D. Zhigadlo, B. Batlogg, A. N. Yaresko, and S. V. Borisenko, Interaction-induced singular Fermi surface in a high-temperature oxypnictide superconductor, *Scientific Reports* 5, 10392 (2015)
- [S17] J. Feng, D. Biswas, A. Rajan, M. D. Watson, F. Mazzola, O. J. Clark, K. Underwood, I. Markovi?, M. McLaren, A. Hunter, D. M. Burn, L. B. Duffy, S. B., G. Balakrishnan, F. Bertran, P. Le Fvre, T. K. Kim, G. van der Laan, T. Hesjedal, P. Wahl, and P. D. C. King, Electronic Structure and Enhanced Charge-Density Wave Order of Monolayer VSe_2 Nano Letters 18, 4493-4499 (2018)
- [S18] K. Tsutsumi, X-ray-diffraction Study of the Periodic Lattice Distortion Associated with a Charge-density Wave in 1T- VSe_2 , *Phys. Rev. B: Condens. Matter Mater. Phys.* 26, 5756? 5759 (1982)
- [S19] D. J. Eaglesham; R. L. Withers, and D. M. Bird, Charge-density-wave Transitions in 1T- VSe_2 . *J. Phys. C: Solid State Phys.* 19, 359 (1986)
- [S20] A. Shtyk, G. Goldstein, and C. Chamon, Electrons at the monkey saddle: A multicritical Lifshitz point, *Phys. Rev. B* 95, 035137 (2017).
- [S21] Y. Sherkunov, J. J. Betouras, Novel phases in twisted bilayer graphene at magic angles as a result of van Hove singularities and interactions, *arXiv:1807.05524* (2018)
- [S22] Y. Cao, V. Fatemi, A. Demir, S. Fang, S. L. Tomarken, J. Y. Luo, J. D. Sanchez-Yamagishi, K. Watanabe, T. Taniguchi, E. Kaxiras, R. C. Ashoori, and Pablo Jarillo- Herrero, Correlated insulator behaviour at half-filling in magic-angle graphene superlattices, *Nature* 556, 80 (2018).
- [S23] Y. Cao, V. Fatemi, S. Fang, K. Watanabe, T. Taniguchi, E. Kaxiras, and Pablo Jarillo- Herrero, Unconventional superconductivity in magic- angle graphene superlattices, *Nature* 556, 43 (2018)
- [S24] Qualitative similar hamiltonians have been previously been postulated previously (e.g. ^{S13}). Here we have followed a more rigorous line of argument starting from the DFT calculation and tight binding model allowing a more precise determination of orbital character and origin of the observed band structure. However qualitatively the hamiltonians are equivalent.